Scaling of surface roughness in film deposition with height-dependent step edge barriers

Ismael S. S. Carrasco [1,*] Tung B. T. To [2,†] and Fábio D. A. Aarão Reis [2,‡]

[1] *International Center of Physics, Institute of Physics, University of Brasilia, 70910-900 Brasilia, Federal District, Brazil*

[2] *Instituto de Física, Universidade Federal Fluminense, Avenida Litorânea s/n, 24210-340 Niterói, Rio de Janeiro, Brazil*

(Received 24 August 2023; accepted 10 November 2023; published 5 December 2023)

We perform kinetic Monte Carlo simulations of film growth in simple cubic lattices with solid-on-solid conditions, Ehrlich-Schwoebel (ES) barriers at step edges, and a kinetic barrier related to the hidden off-plane diffusion at multilayer steps. Broad ranges of the diffusion-to-deposition ratio R, detachment probability per lateral neighbor, ϵ, and monolayer step crossing probability $P = \exp[-E_{ES}/(k_BT)]$ are studied. Without the ES barrier, four possible scaling regimes are shown as the coverage θ increases: nearly layer-by-layer growth with damped roughness oscillations; kinetic roughening in the Villain-Lai–Das Sarma (VLDS) universality class when the roughness is $W \sim 1$ (in lattice units); unstable roughening with mound nucleation and growth, where slopes of $\log W \times \log \theta$ plots reach values larger than 0.5; and asymptotic statistical growth with $W = \theta^{1/2}$ solely due to the kinetic barrier at multilayer steps. If the ES barrier is present, the layer-by-layer growth crosses over directly to the unstable regime, with no transient VLDS scaling. However, in simulations up to $\theta = 10^4$ (typical of films with a few micrometers), low temperatures (small R, ϵ, or P) may suppress the two or three initial regimes, while high temperatures and $P \sim 1$ produce smooth surfaces at all thicknesses. These crossovers help to explain proposals of nonuniversal exponents in previous works. We define a smooth film thickness θ_c where $W = 1$ and show that VLDS scaling at that point indicates negligible ES barriers, while rapidly increasing roughness indicates a small ES barrier ($E_{ES} \sim k_BT$). θ_c scales as $\sim \exp(\text{const} \times P^{2/3})$ if the other parameters are kept fixed, which represents a high sensitivity on the ES barrier. The analysis of recent experimental data in the light of our results distinguishes cases where $E_{ES}/(k_BT)$ is negligible, ~ 1, or $\ll 1$.

DOI: 10.1103/PhysRevE.108.064802

I. INTRODUCTION

The growth of thin solid films has been a topic of intense research in the last decades due to the large number of applications of these materials [1–3]. When the films are produced by vapor deposition with thermal velocities, large oriented crystalline grains may grow if the adsorbed material relaxes to low-energy configurations by diffusive transport. During this relaxation, adsorbed atoms or molecules on grain facets have to overcome activation energy barriers which usually increase at step edges, leading to rates of interlayer transport smaller than those of intralayer transport. The step edge barriers were first recognized in the works of Ehrlich and Schwoebel [4,5], so they are abbreviately termed ES barriers.

The effect of thermal relaxation on the morphology of growing films is described by several models [6–8]. In the simplest cases, energy barriers for adatom hops depend only on the numbers of nearest neighbors (NNs) on the lattice; this is the case, for instance, of the deposition model of Clarke and Vvedensky (CV) [9]. If no ES barrier is present, the films grow with self-affine surfaces [8,10], in which roughness and correlations scale as power laws of the time and of the observation length as predicted by the Villain-Lai–Das Sarma (VLDS) growth equation [11–14]. In the presence of ES barriers, the limited interlayer transport leads to much faster roughening and mound formation [6]. Several models also considered downward funneling (DF) of the incoming atoms or other mechanisms of transient mobility that lead to mound coarsening [7]. However, no universal picture of the roughening with ES barriers was obtained yet, as recently discussed by Schneider *et al.* [15].

An additional problem appears in models based on simple cubic (SC) lattices and on the solid-on-solid (SOS) condition, which precludes the formation of overhangs in the deposition direction. Consider, for instance, the adatom hops from A to A′ and from B to B′ shown in Fig. 1(a). The rotated image of Fig. 1(b) suggests that a displacement from A to A′ requires a diffusive motion on a [100] terrace after the adatom crosses the step edge; this differs from the displacement from B to B′, which only requires the crossing event. The [100] terrace is physically equivalent to the [001] terraces, but adatom diffusion on [100] (and [010]) terraces cannot be explicitly represented in SOS models because overhangs would be formed. To account for that out-of-plane diffusion process, Leal *et al.* [16] proposed a one-dimensional random walk that reduces the hopping probability by a factor dependent on the height difference between the initial and final points [see Eq. (4) in the next section]. In this model, a kinetic barrier originating from the hidden out-of-plane diffusion is combined with the ES barrier.

*ismael.carrasco@unb.br
†tobathanhtung@gmail.com
‡fdaar@protonmail.com

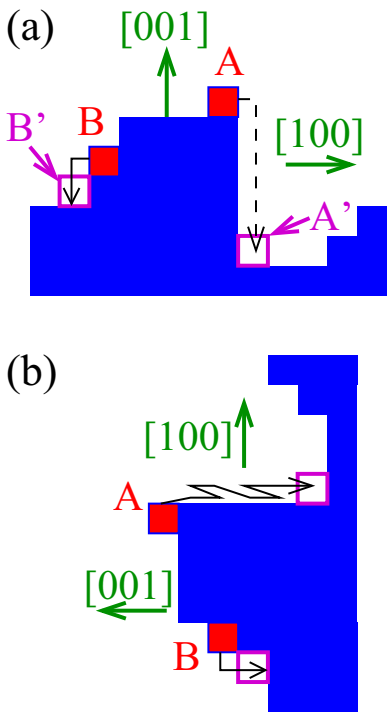

FIG. 1. (a) Two adatoms at positions A and B (red) hop to positions A′ and B′ (open magenta squares). The other adatoms of the film are in blue. (b) The same sample rotated 90° to the left shows that the adatom hop from A to A′ represents the step edge crossing and the diffusion on a [100] plane.

Formerly, the study of homoepitaxial growth with this kinetic barrier also considered DF of the incident atoms [16]. Simulations without the ES barrier showed VLDS scaling with very small roughness, and simulations with the ES barrier showed a time increase of the roughness as $\sim t^{1/3}$. In recent applications to the early stages of heteroepitaxial film growth, the combination of those barriers was also considered [17,18]. However, no universal picture of kinetic roughening regimes emerged from those works.

The present work fills this gap by studying a minimal model that includes the ES barrier and the kinetic barrier generated by the hidden out-of-plane diffusion in simple cubic lattices. Surface relaxation is described as in the CV model, with no mechanism of transient mobility after atom adsorption. In the growth without the ES barrier, our kinetic Monte Carlo simulations show four possible scaling regimes depending on the interplay of the material energetic, the growth temperature, and the film thickness: damped layer-by-layer growth, kinetic roughening in the VLDS class [11,12], unstable roughening with mound nucleation and growth, and statistical growth (SG) with roughness scaling as $W = t^{1/2}$ [6,7]. When the ES barrier is present, no evidence of a VLDS regime is found and the onset of unstable roughening has a remarkable sensitivity on that barrier. The scaling relations of the roughness and of correlation lengths obtained here are similar to those of some recently studied materials, and the transition from layer-by-layer growth to a linear time scaling of the roughness, obtained with small ES barriers, is in qualitative agreement with that of diindenoperylene (DIP) films deposited on SiO_2 [19].

II. MODEL AND METHODS

A. Deposition model

The deposit has a SC structure with sites of edge a and all measured lengths are given in units of a. The flat substrate is located at $z = 0$ and substrate atoms are immobile. Each deposited atom or molecule occupies a single lattice site at $z \geqslant 1$. For simplicity, they are hereafter termed adatoms, although applications to molecular films will be discussed. Periodic boundary conditions are considered in the x and y directions. Solid-on-solid conditions were considered, so the deposits have no pores. The set of adatoms with the same (x, y) position is termed a column of the deposit and the height variable $h(x, y)$ is the z coordinate of the topmost adatom in that column.

The atomic flux is collimated in the $-z$ direction with a rate of F atoms per substrate site per unit time. A column (x, y) is randomly chosen for each incident atom, which adsorbs as it lands at the top of that column. Desorption is neglected in our model.

The adatoms at the top of the columns may execute surface diffusion, while those located below the column tops are immobile (but they become mobile if the adatoms above them hop to other columns). When an adatom attempts to hop, the target direction is randomly chosen among the four NN columns, $\pm x$ or $\pm y$. The rate of an intralayer hop (i.e., hop without change in the z position) of an adatom with n lateral NNs is

$$D = D_0 \epsilon^n, \tag{1}$$

where D_0 is a terrace diffusion coefficient

$$D_0 = \nu \exp\left[-E_S/(k_B T)\right] \tag{2}$$

and

$$\epsilon \equiv \exp\left[-E_B/(k_B T)\right] \tag{3}$$

is a detachment factor (corresponding to detachment from lateral NNs). Here, ν is a frequency, while $E_S > 0$ and $E_B > 0$ are activation energies, k_B is the Boltzmann constant, and T is the substrate temperature.

Interlayer adatom hops have the rates of Eq. (1) multiplied by a probability $P_{\rm hop}$, which incorporates the ES barrier and the kinetic barrier related to out-of-plane adatom diffusion [Fig. 1(b)]. Following the reasoning of Ref. [16], we consider

$$P_{\rm hop} = \frac{P}{1 + P(\Delta h/a - 1)}, \quad P = \exp\left[-E_{ES}/(k_B T)\right], \tag{4}$$

where E_{ES} is the ES energy barrier. With this form, $P_{\rm hop} = P$ is recovered in monolayer steps ($\Delta h = a$), which is the case of the hop from B to B′ in Fig. 1(b). The same probability $P_{\rm hop}$ is considered for downward and upward motion; thus, the full set of adatom hopping rules satisfies detailed balance conditions.

The deposition and the diffusion of some adatoms are illustrated in Fig. 2, with the corresponding rates. The hopping rates on the substrate and on the deposit are the same. This is a typical assumption for homoepitaxial growth, but the results obtained after the deposition of several atomic or molecular layers do not depend on this initial condition and may also be compared with results of heteroepitaxial growth.

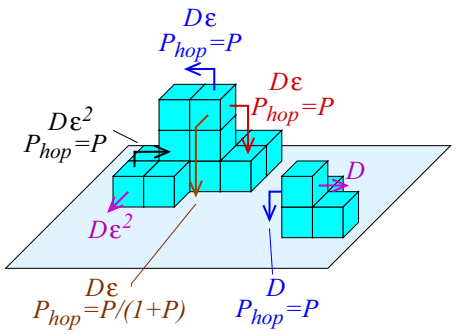

FIG. 2. Possible hops (arrows) of some adatoms (light blue) with hopping rates of the form $D\epsilon^n$ and hopping probabilities $P_{\rm hop}$ for crossing step edges; intralayer hops have $P_{\rm hop} = 1$ (not shown). Observe that the hopping rates depend only on the adatom neighborhood while the hopping probabilities depend on the target site of the hop.

For a given deposited material, the set of activation energies is constant. The deposition conditions are then characterized by three dimensionless parameters: the detachment factor ϵ [Eq. (3)], the ES probability P [Eq. (4)], and the diffusion-to-deposition ratio on terraces,

$$R = \frac{D_0}{F} = \tilde{\nu}\exp\left[-E_S/(k_B T)\right], \tag{5}$$

where $\tilde{\nu} = \nu/F$. At high temperatures, the average number of hops of an adatom (predominantly on large terraces) is proportional to R, but slower scaling with this parameter is found at low temperatures [20].

Previous works on deposition models with the kinetic barrier of Eq. (4) also considered downward funneling (DF) of incident atoms, in which they are scattered to NN columns with smaller heights or with higher coordination [16,21]. Such mechanisms allow the incident atoms to bypass the barriers at high multilayer steps. However, our aim is to distinguish the universal effects of the step edge barriers, so we do not consider those transient mobility mechanisms.

B. Quantities of interest

The dimensionless film thickness (or coverage) is denoted as

$$\theta = Ft. \tag{6}$$

This is the average number of deposited atoms per column at time t, or number of deposited layers.

The surface fluctuations are characterized by the film's roughness

$$W = \sqrt{W_2} = \langle(\overline{\tilde{h}^2})\rangle^{1/2}, \quad \tilde{h} \equiv h - \overline{h}, \tag{7}$$

where the overbars denote a spatial average over the whole sample and the angular brackets denote an average over different configurations with a given thickness.

In kinetic roughening processes in wide substrates, the roughness is expected to scale as

$$W \sim \theta^{\beta}, \tag{8}$$

where β is called the growth exponent. This scaling may be investigated with the calculation of local slopes of the $\log W \times \log\theta$ plots, which are defined as effective growth exponents:

$$\beta_{\rm eff} = \frac{{\rm d}(\log W)}{{\rm d}(\log\theta)}. \tag{9}$$

From simulation data, $\beta_{\rm eff}$ is calculated in appropriately chosen time intervals, which must be large enough to reduce the effect of statistical fluctuations in W but small compared to the total simulation times.

The spatial correlations along the surface can be characterized by the autocorrelation function Γ. At a distance s, it is defined as [22]

$$\Gamma(s) = \frac{\langle\tilde{h}(\vec{r}_0)\tilde{h}(\vec{r}_0+\vec{s})\rangle}{W_2}, \qquad s \equiv |\vec{s}|, \tag{10}$$

where W_2 is given in Eq. (7) and the configurational average is taken over different initial positions $\vec{r}_0$, different orientations of $\vec{s}$ (directions x and y), and different deposits. At any time, $\Gamma = 1$ for $s = 0$.

The correlation of height fluctuations may be characterized by the correlation length ξ defined by [22]

$$\Gamma(\xi) = e^{-1} \approx 0.3679. \tag{11}$$

In kinetic roughening processes, this length is expected to scale as

$$\xi \sim \theta^{1/z}, \tag{12}$$

where z is the dynamical exponent.

In mounded surfaces, the average mound size is approximately twice the position λ of the first minimum of the autocorrelation function [22]:

$$\left.\frac{d\Gamma}{ds}\right|_{\lambda} = 0. \tag{13}$$

Here we do not discuss additional quantities because they may have crossovers that impair the physical interpretations, as shown in recent studies of height distributions of the CV model [23] and of surface fractal dimensions of limited mobility models [24].

C. Basics of kinetic roughening

In order to describe growth dominated by adatom surface diffusion in the hydrodynamic limit, Villain, Lai, and Das Sarma [11,12] proposed the so-called VLDS equation

$$\frac{\partial h(\vec{r},t)}{\partial t} = \nu_4\nabla^4 h + \lambda_4\nabla^2(\nabla h)^2 + \eta(\vec{r},t), \tag{14}$$

where $h(\vec{r},t)$ is the height at position $\vec{r}$ and time t in a d-dimensional substrate, ν_4 and λ_4 are constants, and η is a Gaussian, nonconservative noise. The contribution of the average external flux is omitted in Eq. (14).

The VLDS equation provides a coarse-grained representation of several lattice models in which adatom diffusion controls the surface relaxation; the corresponding coefficients ν_4 and λ_4 and the noise amplitude depend on the rules of each model. Such models are said to belong to the VLDS universality class. In three dimensions ($d = 2$), the best numerical estimates of scaling exponents of this class are $\beta \approx 0.20$ and $z \approx 3.3$ [14,25–27], which agree with two-loop renormalization estimates $\beta \approx 0.199$ and $z \approx 3.36$ [28].

TABLE I. Parameter sets used in the simulations. The last column corresponds to the maximal E_{ES} used, corresponding to $P = 0.01$.

Set	E_S (eV)	E_N (eV)	T (K)	R	ϵ	Max E_{ES} (eV)
A	0.667	0.166	300	6.3×10^2	0.0016	0.119
B	0.667	0.133	300	6.3×10^2	0.0058	0.119
C	0.725	0.164	350	3.6×10^3	0.0043	0.139
D	0.725	0.131	350	3.6×10^3	0.013	0.139
E	0.805	0.266	400	7.2×10^3	0.00044	0.159
F	0.805	0.133	400	7.2×10^3	0.021	0.159
G	0.839	0.188	450	4.00×10^4	0.0079	0.179
H	0.839	0.150	450	4.00×10^4	0.021	0.179
I	0.923	0.333	500	4.98×10^4	0.00044	0.198
J	0.923	0.170	500	4.98×10^4	0.021	0.198
K	0.954	0.210	550	1.80×10^5	0.012	0.218
L	0.831	0.366	550	2.38×10^6	0.00044	0.218
M	0.908	0.200	600	2.38×10^6	0.021	0.238

The CV model without step edge barriers [i.e., $P_{\text{hop}} = 1$ in Eq. (4)] is theoretically predicted to belong to the VLDS class [29], which is confirmed by simulations [13,14,30]. Simulations in a broad range of parameters confirm this prediction and show that the roughness can be written as [13]

$$W = f_{CV}\left(\frac{\theta}{R^{3/2}[\epsilon + c]}\right), \tag{15}$$

where f_{CV} is a function that scales as $f_{CV}(x) \sim x^{0.20}$ for $x \gg 1$ (i.e., $\beta \approx 0.20$) and $c \approx 0.025$.

When the film growth occurs without interlayer transport, the roughness scales as [6]

$$W = \theta^{1/2} \tag{16}$$

(i.e. $\beta = 1/2$), which is termed statistical growth (SG).

There are also cases of unstable roughening in which the surface peaks grow faster than the valleys. If different growth velocities persist at long times, the height fluctuations linearly increase in time, i.e., with $\beta = 1$.

D. Simulation parameters

Table I shows the sets of parameters of the CV model used in the simulations, which are labeled from A to M. In order to choose these sets, we first choose values of ν, F, E_S, and E_B. The typical value $\nu = 10^{13}$ s^{-1} and a small flux $F = 0.1$ s^{-1} give $\tilde{\nu} = 10^{14}$ in Eq. (5). The energy values that describe the growth of metal and semiconductor films generally obey the relation $E_S > E_B$, so this relation is obeyed in all simulated sets. Since our aim is to scan a broad range of deposition conditions, we attempted to vary the dimensionless parameters R and ϵ by some orders of magnitude; consequently, for most energy sets, simulations in only one temperature were performed.

The values of E_{ES} used in the simulations of each parameter set varied between zero (no ES barrier, $P = 1$) and the maximal value listed in Table I. The strongest ES barrier in all cases corresponds to $P = 0.01$.

The maximal film thickness is $\theta = 10^4$ in most parameter sets. For deposition of atoms or molecules with diameters typically in the range 0.2–2 nm, the maximal simulated thicknesses are roughly 2–20 μm. The only exceptions are sets A, B, and C, in which simulations up to $\theta = 10^6$, 10^5, and 10^5 were performed, respectively. For each parameter set, the number of generated deposits varied from 10 to 100.

The fluctuations of the average quantities among the simulated deposits were small, as shown in Appendix A. This justifies the relatively small number of configurations used for the averaging. Moreover, it shows that the uncertainties of the data points are sufficiently small to justify not plotting the error bars throughout this work.

The lateral size of the substrate and of the simulated deposits is $L = 1024a$. It was checked to be large enough to avoid finite-size effects on the calculated quantities, as shown in Appendix B.

The simulations were implemented with the kinetic Monte Carlo (KMC) algorithm described in detail in Ref. [31] and summarized in Appendix C.

III. RESULTS

The presentation of results hereafter refers to model parameters by the labels in Table I [from A to M, which set the pair (R, ϵ)] and to the value of P.

A. Growth with large ES barriers

Here we analyze the results of simulations with $P = 0.01$, which corresponds to $E_{ES} \approx 5k_BT$ (the maximal values of E_{ES} in Table I).

Figure 3 shows top and cross-section views of a film grown with the parameter set M and four thicknesses. This is the set with the highest adatom mobility studied here. Islands nucleate at the substrate and give rise to mounds, which continuously grow vertically but have little change in their lateral sizes. Thus, the dynamics of the formation of the first layers control the mound size. Similar features are observed for other parameters sets, though with smaller islands. A notable feature at the longest times is the formation of ridges aligned in $(\pm 1, \pm 1, 0)$ directions, which is a consequence of a slow coarsening of neighboring mounds.

Figure 4(a) shows W as a function of θ in films grown with sets F, I, and M, which span more than two orders of magnitude of R and two values of ϵ. In all cases, the roughness follows a power-law relation with slope ≈0.5 as in SG [Eq. (16)]. However, the prefactors of that relation are 0.6–0.8 in the thickest films, $\theta \sim 10^4$. This is consistent with negligible mass flux between the mounds, which leads to an effectively random (uncorrelated) deposition [10] at the scale of the mound size.

Figure 4(b) shows the autocorrelation function of films grown with set I with thicknesses from 10 to 10^4. The small differences between the curves indicate that the associated correlation lengths ξ and λ increase very slowly in time. This confirms the negligible coarsening of mounds. The formation of ridges, shown in Fig. 3, does not affect those characteristic lengths because those structures are elongated in only one direction.

The main features discussed above were already observed in homoepitaxial growth models with strong ES barriers but

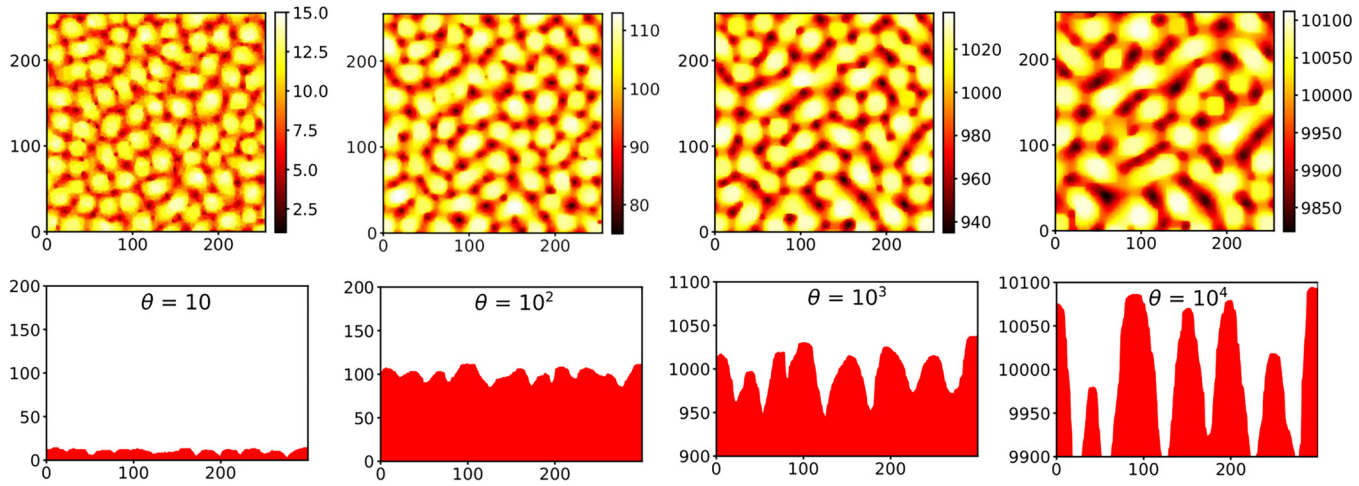

FIG. 3. Vertical cross sections and top views of parts of the deposits grown in simulations with set M and $P = 0.01$. All lengths are in units of the lattice constant.

without the kinetic barrier. In heteroepitaxial growth, if the substrate effects disappear after the formation of a continuous film, the mounds will grow with the same sizes as in the present model. However, in such cases, the adatom diffusion coefficient on the substrate differs from that on the film surface, which may lead, e.g., to growth of islands on the substrate. These initial growth features, including the nontrivial variations of the roughness when the islands coalesce, were analyzed in recent works [17,18].

B. Growth with the kinetic barrier only ($E_{ES} = 0, P = 1$)

1. Evolution of film morphology

Figures 5(a)–5(c) show top and cross-section images of deposits grown with parameter sets A, F, and M, comprising three orders of magnitude of the thickness. Set A is the case with the lowest adatom mobility. When the film has small numbers of layers ($\theta = 10$–10^2), the surface only shows some asperity, but at $\theta \sim 10^3$ it has mounds of irregular shape separated by narrow gaps. This irregular mound pattern develops deeper gaps in the largest thicknesses ($\theta \sim 10^4$). For the intermediate values of R and ϵ, the parameter set F [Fig. 5(b)] produces smooth surfaces from 10 to 10^4 deposited layers.

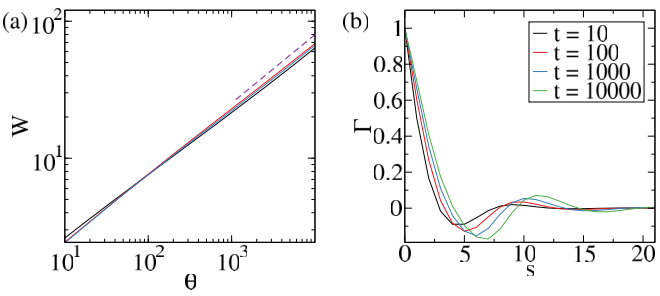

FIG. 4. (a) Evolution of the surface roughness of films grown with sets F (black), I (red), and M (blue), with the highest ES barriers ($P = 0.01$). The dashed line is the SG of Eq. (16). (b) Autocorrelation function of films grown with set I and $P = 0.01$ at the indicated times. All lengths are in units of the lattice constant.

At $\theta = 10$, the surface has a wide terrace with shallow valleys and monolayer islands with disordered borders. In the thickest films ($\theta = 10^3$–10^4), wide mounds and shallow valleys are formed [respectively yellow and black tones in Fig. 5(b)], whose lateral sizes are apparently increasing in time. When the film is grown with the largest adatom mobilities [set M, Figs. 5(c)], wide terraces appear until the largest thicknesses, while monolayer valleys and islands have smooth borders.

2. Surface roughness

Figure 6(a) shows the evolution of the surface roughness in films with small thicknesses ($\theta \leqslant 30$) grown with five parameter sets. In films grown with $R > 10^3$ (all sets except A and B), oscillations are observed when the roughness is 0.5 or smaller, which indicates approximately layer-by-layer growth. As the adatom mobility increases, the oscillations persist at longer times; in sets L and M, they are observed until $\theta > 10^2$. During the oscillations, the maxima $W \approx 0.5$ are obtained nearly at half-integer θ. The minima are obtained nearly at integer θ and are typically above $W \approx 0.2$, which means that perfectly flat surfaces are not obtained in those conditions. The oscillations are damped because the minima of W increases as the film grows, indicating that the deviation from the perfect filling increases.

Figure 6(b) shows W in the whole range of θ of the simulations with the same parameter sets. For better visualization, the plots are built with constant intervals of $\log\theta$ between consecutive data points, so the initial roughness oscillations may be hindered or distorted in some cases. Figure 6(c) shows the evolution of the corresponding effective growth exponents [Eq. (9)].

In the films grown with set A, the small roughness at $\theta \lesssim 10^2$ is consistent with the smooth surfaces observed in Fig. 5(a). Subsequently, W grows with increasing slope β_{eff} until $\sim 10^4$ layers. This suggests unstable roughening, which physically corresponds to the formation of the mounds of irregular shape separated by deep gaps, as shown in Fig. 5(a). However, the effective exponent β_{eff} decreases for larger thicknesses, which means that the unstable growth is also

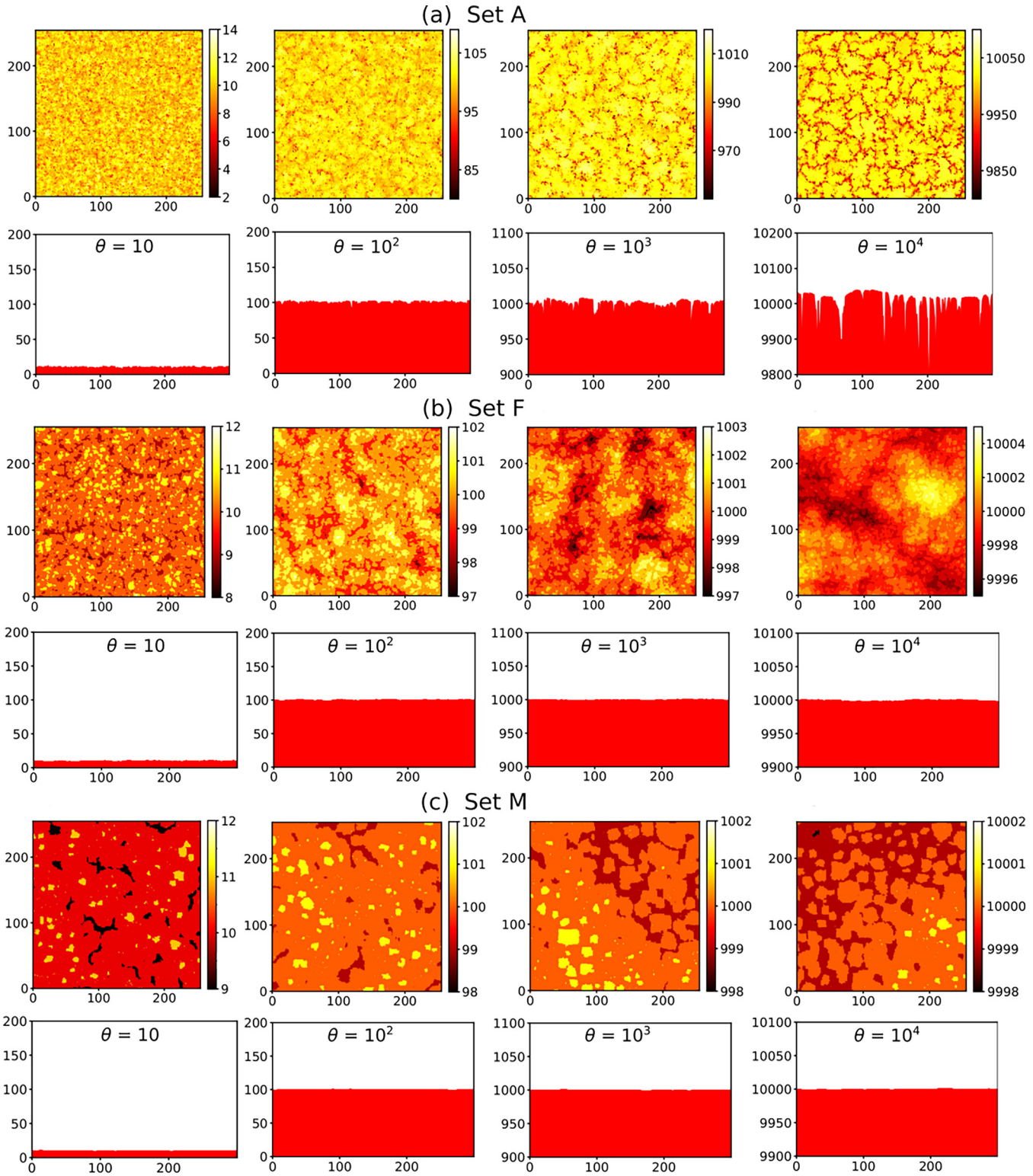

FIG. 5. Top and cross-section views of parts of the deposits grown with sets (a) A, (b) F, and (c) M with $P = 1$. All lengths are given in lattice units.

transient. The convergence to the exponent 0.5 of SG [Eq. (16)] is suggested in Fig. 6(c).

The films grown with set C have small roughness until $\theta \sim 10^4$, but the roughening is much faster in the subsequent time or thickness decade. This is confirmed by the rapid increase of β_{eff}, which reaches values much larger than 0.5. Compared with set A, these results show that the higher adatom mobility of set C delays the instability, but it becomes more pronounced. In the largest thicknesses, β_{eff} begins to decrease.

These features are consistent with the expectation of a universal SG asymptotically. Additional support is provided by the evolution of the adatom current, which tends to zero at

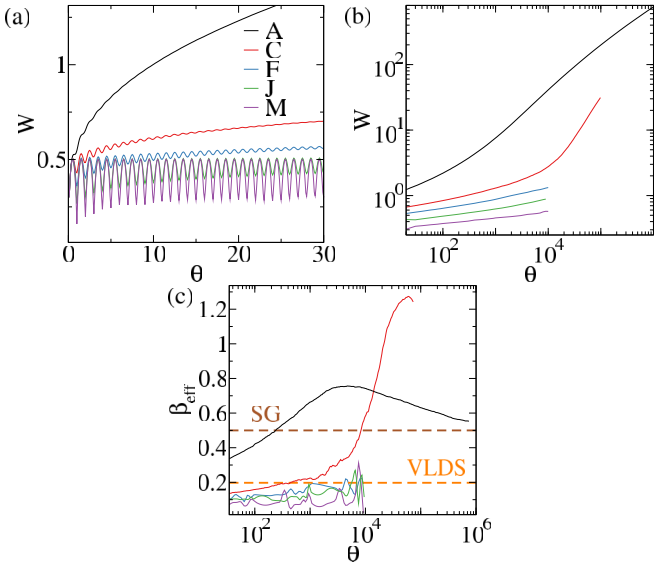

FIG. 6. Evolution of (a) surface roughness at short times, (b) surface roughness at all simulated times, and (c) effective growth exponent of films grown with sets A (black), C (red), F (blue), J (green), and M (purple), with $P = 1$. All lengths are in units of the lattice constant.

long times, as shown in Appendix D. Such an expectation is reasonable because the symmetries of the interactions are the same for all values of the model parameters.

The films grown with set F have small roughness (between 1 and 2) until $\theta \sim 10^4$ and the exponents $\beta_{\rm eff}$ slowly increase. In the films grown with sets J and M, the oscillations of the roughness are followed by a slow increase of that quantity. The large fluctuations in $\beta_{\rm eff}$, particularly in set M, are consequences of the large relative fluctuations of W. From the point of view of applications, an important consequence of these results is that, without the ES barrier, the asymptotic SG can hardly be observed up to 10^4 deposited layers, which typically means a thickness of a few micrometers.

3. Correlation lengths

Figure 7(a) shows the correlation length ξ [Eq. (11)] and Fig. 7(b) shows the length λ [Eq. (13)] as functions of the thickness for the same parameter sets of Figs. 6(a)–6(c). In both plots, the dashed lines have the slope 0.30 of the correlation length of the VLDS class, which is the class of the CV model without step edge barriers.

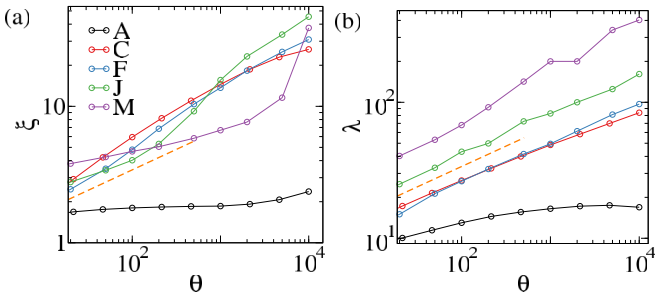

FIG. 7. Evolution of (a) correlation length ξ and (b) characteristic length λ of films grown with sets A (black), C (red), F (blue), J (green), and M (purple), with $P = 1$. In (b), the dashed line has the slope 0.30 of the correlation length in the VLDS class. All lengths are in units of the lattice constant.

In films grown with set A, both lengths slowly vary in time; a similar result is obtained with set B. This is consistent with the absence of coarsening of the mounds shown in Fig. 5(a) due to the limited interlayer transport. Combined with the trend of decrease of $\beta_{\rm eff}$ in Fig. 6(c), these results confirm the asymptotic SG as a consequence of the kinetic barrier alone.

The evolution of the correlation length ξ is very different for different parameter sets. The $\log\xi \times \log\theta$ plots of films grown with sets C and F have downward curvatures, so reliable scaling exponents cannot be obtained; in set J, the plot changes the curvature between $\theta = 10^2$ and 10^3, and in set M, ξ has very slow variation with the thickness (except for a bump in the thickest samples).

On the other hand, the slopes of the $\log\lambda \times \log\theta$ plots are near the VLDS value 0.30 across three orders of the thickness in sets C, F, J, and M. Similar behavior is observed in films grown with other parameter sets. There is no mound formation in those films up to $\theta = 10^4$, so we understand that the increase of λ is representing an increase in the distance of neighboring peaks and valleys which have small height differences.

4. Scaling relations

The features of films with small roughness, especially in the regime of layer-by-layer growth, can be explained by recalling results of previous studies of submonolayer growth [32–35]. This is possible because the surface dynamics is mainly controlled by a top layer above some completely filled layers. First, in set M, $\epsilon R^{1/5} \sim 1$ corresponds to a high-temperature regime in which four-adatom islands on terraces may be unstable [35]. This explains the persistence of roughness oscillations until large thicknesses and, after the oscillations are damped, the very slow increase of the roughness [Figs. 6(a) and 6(b)]. The same studies of submonolayer growth show that two-adatom islands are stable for $\epsilon R^{2/3} < 1$, while their instability is expected if $\epsilon R^{2/3} \gtrsim 10$ [35]. The former condition is observed in sets A and B, the latter is observed in sets F–M, and sets C–E are in a crossover region. The instability of two-adatom islands allows the formation of large islands on terraces, which facilitates the layer-by-layer growth. This explains why long roughness oscillations are also shown in sets F–L [see data for F and J in Fig. 6(a)]. Instead, the stability of two-adatom islands with the parameter sets A and B implies almost irreversible aggregation of adatoms to existing islands; thus, at short times, adatoms may be at stable positions in several layers, which leads to surface roughening instead of layer-by-layer growth.

As the films grow, the kinetic barrier is expected to play a role when a significant fraction of the neighboring columns have height differences >1 (in units of the lattice constant). We expect that this occurs when $W \gtrsim 1$. When $W \sim 1$, the effect of the kinetic barrier is still negligible, so the roughness is expected to vary approximately as in the CV model without step edge barriers, Eq. (15). Of course this is applicable after the layer-by-layer regime with $W \lesssim 0.5$, so it is applicable to a very narrow range of roughness.

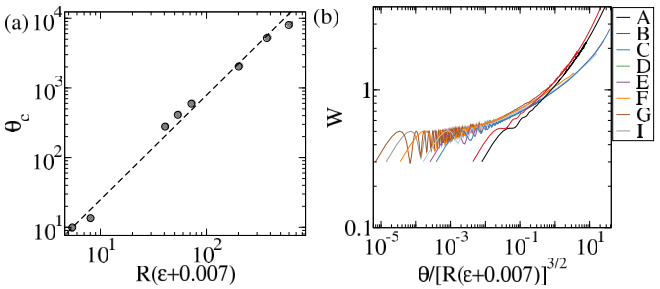

FIG. 8. (a) Scaling of the characteristic thickness of smooth films for the indicated parameter sets with $P = 1$. (b) Surface roughness as a function of the scaled thickness for the indicated parameter sets with $P = 1$. All lengths are in units of the lattice constant.

In order to investigate the consistency of this interpretation, we define the characteristic thickness θ_c of smooth films by

$$W(\theta_c) = 1. \tag{17}$$

Assuming that the roughness follows Eq. (15), we expect that $\theta_c \sim R^{3/2}(\epsilon + c)$, with c constant. Figure 8(a) shows that θ_c is a function of a slightly changed variable $R(\epsilon + 0.007)$, with the dashed line of slope 3/2 in the double logarithmic plot. This leads to

$$\theta_c \sim [R(\epsilon + 0.007)]^{3/2}, \tag{18}$$

i.e., the same power law on R obtained in the CV model without step edge barriers [13], but a slightly different dependence on ϵ. This confirms that a transient VLDS regime is present when the roughness is small.

The transient VLDS scaling is also supported by the former results for the roughness and for the length λ. The exponents β_{eff} in Fig. 6(c) are near the VLDS value ≈0.20 in films grown with sets C and F when $W \approx 1$. Moreover, the length λ in Fig. 7(b) scales with an exponent near the VLDS value ≈0.30. Interestingly, the VLDS regime is indicated by a length that characterizes typical distances of peaks and valleys, in contrast with the correlation length ξ.

In Fig. 8(b), we show the film roughness as a function of the scaled thickness $\theta/[R(\epsilon + 0.007)]^{3/2}$ for several parameter sets. The data for most sets collapse into a universal curve whose slope rapidly increases for $\theta \gtrsim \theta_c$; this indicates a crossover from the VLDS regime to unstable roughening. The deviations from the collapse in sets A and B are probably related to their small values of θ_c and consequent narrow range of the VLDS transient. On the other hand, it is interesting to observe that the oscillations of W in some sets behave as wrappings of the universal curve of Fig. 8(b).

C. Growth with small ES barrier

Now we study the growth with small ES barriers, $0.1 \leqslant P \leqslant 0.8$, corresponding to E_{ES} between $\approx 0.2 k_B T$ and $\approx 2.3 k_B T$.

1. Surface morphology

The snapshots of a film in Fig. 9 were obtained with set F and $P = 0.4$ ($E_{ES} \approx k_B T$). For small thickness, $\theta = 10$, the film surface is relatively smooth. The comparison with the films grown with $P = 1$ [Fig. 5(b)] shows no relevant difference in the morphology. When $\theta = 10^2$, the top view shows the nucleation of mounds separated by narrow gaps in films grown with the ES barrier. However, the cross-section view shows that the surface is globally smooth; i.e., the mounds have very small slopes. When $\theta = 10^3$, the mounds become larger and the gaps between them are deeper, so that the mounded morphology is also visible in the cross-section view. Finally, in the largest thickness, those mounds have grown vertically, but with negligible increase of the lateral size, which indicates that mound coarsening is very slow. This is consistent with a convergence to SG, as observed with larger ES barriers (Sec. III A). These features contrast with those of films grown with set F and $P = 1$, which have smooth surfaces until $\theta = 10^4$ [Fig. 5(b)].

2. Roughness and correlation length

Figure 10(a) shows the short-time evolution ($\theta \leqslant 20$) of the roughness in films grown with $P = 0.1$, the same sets of R and ϵ of Fig. 6(a), and the additional set L. The films grown with sets A, C, and F reach $W = 0.6$ before the deposition of a single layer ($\theta = 1$), so no oscillation is observed. With set J, damped oscillations of the roughness are observed in the first two to three layers and are followed by a rapid increase. With

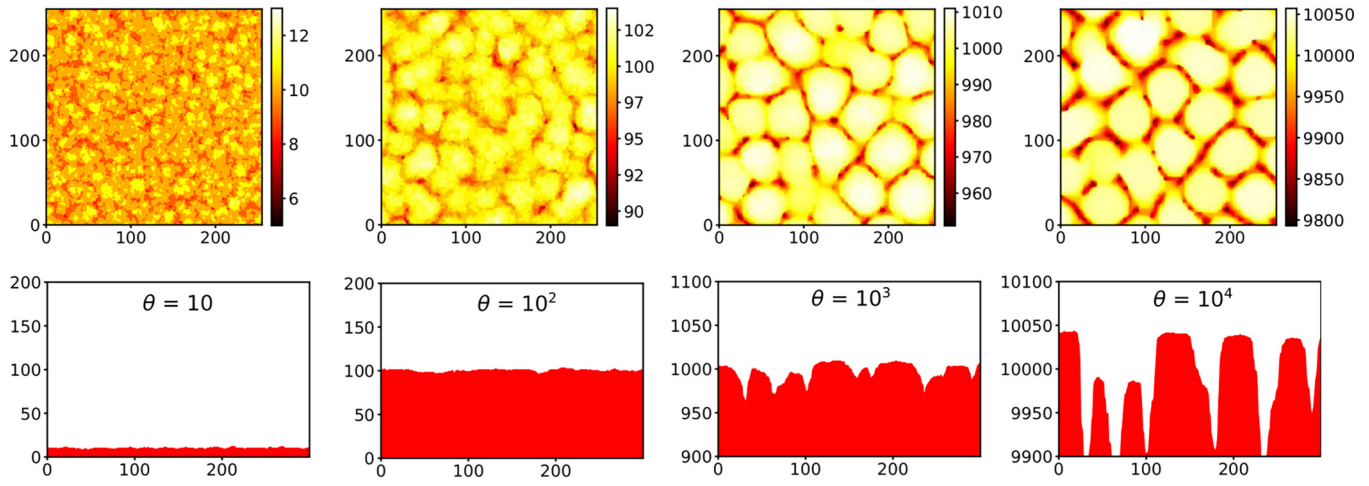

FIG. 9. Top and cross-section views of parts of a deposit grown with set F and $P = 0.4$. All lengths are given in lattice units.

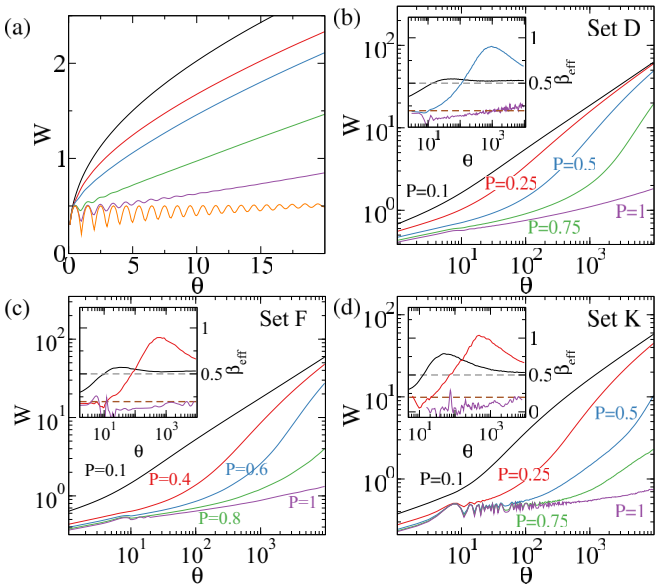

FIG. 10. Surface roughness of films grown with (a) sets A (black), C (red), F (blue), J (green), L (purple), and M (orange) with $P = 0.1$ at short times and sets (b) D, (c) F, and (d) K with several P until $\theta = 10^4$. All lengths are in units of the lattice constant.

set M, the oscillations remain after the deposition of more than 20 layers. For comparison, the oscillations are damped much faster in films grown with set L, in which R is the same as set M but ϵ is smaller (see Table I). These trends show that nearly layer-by-layer growth is facilitated if the adatom mobility is sufficiently high on terraces and at island borders, where the detachment factor ϵ becomes important.

Figures 10(b), 10(c), and 10(d) show the full roughness evolution of films grown with sets D, F, and K, respectively, for P ranging between 0.1 and 1 (different values of P were chosen in each case). The insets of those plots show the evolution of $\beta_{\rm eff}$ for selected values of P. When $W \lesssim 0.5$, i.e., in the conditions of layer-by-layer growth, the difference between the growth with or without the ES barriers is always small. However, after that regime, small changes in P lead to large changes in the roughness evolution; as P decreases, the unstable roughening begins at shorter times. The effect of changing P is observed even when $W \sim 1$, i.e., when the surface is very smooth, because the ES barrier is active at any surface step, contrary to the kinetic barrier, which is active only for height differences 2 or larger. Thus, the crossover thickness θ_c [Eq. (17)] is drastically affected by changes in P, as will be discussed in Sec. III C 3.

The general trend of the roughening can be understood by simultaneous inspection of the snapshots of Fig. 9 and the roughness evolution in Fig. 10(c) for $P = 0.4$. When $\theta = 10^2$ and the mounds are nucleated, the roughness is $\approx$1; i.e., this is close to the smooth film thickness of Eq. (17). The mounded morphology differs from the self-affine morphology of interfaces in the VLDS class, so a transient VLDS scaling is not expected in this case. As the film grows to $\theta = 10^3$, the roughness increases to $\approx$10 and the presence of mounds is clearer. The thickness interval 10^2–10^3 is where the peak in $\beta_{\rm eff}$ is observed, i.e., the region with the faster roughening,

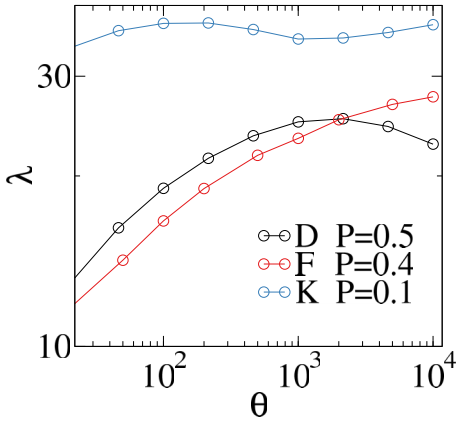

FIG. 11. Characteristic length λ in the indicated sets, given in units of the lattice constant.

which indicates the development of an instability. Similar features are observed with other values of $P < 1$ in different sets. In the largest simulated thicknesses, the trend of $\beta_{\rm eff}$ to converge to the SG value is observed in several cases. The evolution of the adatom current shown in Appendix D and the expectation of universality support the asymptotic SG for all parameter values.

A common feature of all films grown with $P < 1$ is that $\beta_{\rm eff} \gtrsim 0.5$ when $W \sim 1$. This is additional evidence that no transient VLDS regime occurs when the ES barrier is present. Thus, for high adatom mobility, the initial layer-by-layer growth crosses over directly to the unstable growth. Indeed, in that initial regime, as the islands at the top layer become sufficiently wide, the ES barrier prevents the interlayer transport, leading to second-layer island nucleation, as quantitatively explained in Ref. [36].

Figure 11 shows the evolution of the length λ of films grown with three parameter sets that lead to similar evolution of the surface roughness in Figs. 10(a)–10(c). In particular, $W \sim 1$ at $\theta = 10^2$ in all cases and the peak of $\beta_{\rm eff}$ (the signature of the instability) occurs between $\theta = 10^2$ and 10^3. In this region, λ slowly varies; for instance, for set F and $P = 0.4$, λ increases by a factor of ∼1.5, consistently with the widening of the mounds in Fig. 9. In the last decade of time or thickness, all plots show a trend of saturation, indicating that mound coarsening does not occur.

3. *Characteristic thickness of smooth films*

Here we also define the characteristic thickness of smooth film surface using Eq. (17). Our interpretation is that θ_c indicates the onset of mound growth instead of a VLDS regime, which was the case only without the ES barrier.

Figure 12 shows $\ln(\ln\theta_c)$ as a function of $\ln P = -E_{ES}/(k_B T)$ for several parameter sets. The double exponential form is suggested by the high sensitivity of θ_c to variations in P, in contrast with the power-law relations obtained in $P = 1$. In Fig. 12, the plots for constant values of R and ϵ are fit by straight lines that lead to

$$\theta_c \approx \exp\left(BP^{2/3}\right), \tag{19}$$

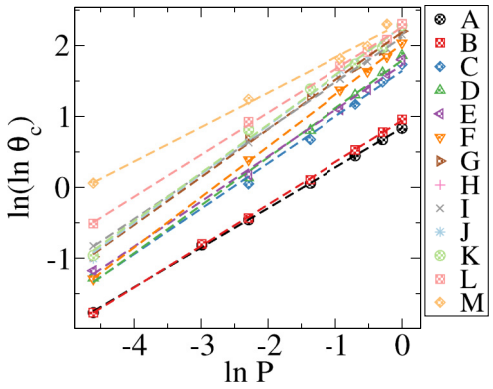

FIG. 12. Characteristic thickness of smooth films as a function of the ES barrier probability in films grown with several parameter sets. Dashed lines are linear fits for each set, i.e., constant R and ϵ.

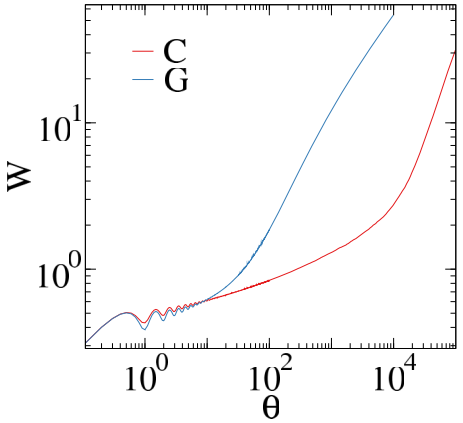

FIG. 13. Evolution of the roughness in films grown with set C and $P = 1$ (red) and set G and $P = 0.25$ (blue). All lengths are given in lattice units.

where B is a constant that depends on those parameters. Deviations are observed only in growth with relatively low adatom mobility (sets A and B) and with the highest mobilities (sets L and M), in which the exponents of P in Eq. (19) change to values $\approx$0.5.

Observe that R and ϵ depend on the temperature as well as the parameter P, so the interpretation of the fits in Fig. 12 and of Eq. (19) must be careful. For instance, if one attempts to interpret them as Arrhenius plots (in which the variable in the abscissa changes with the temperature), then the temperature variation has to be so small that variations in R and ϵ can be neglected, but not the variation in P.

The scaling relation (18) is not expected with $P < 1$ because there is no evidence of a transient VLDS scaling. Indeed, if W is plotted as a function of θ/θ_c, no data collapse is obtained. We also tried to extend the scaling plot of Fig. 8(b) by including corrections in the form $\exp(P^\alpha)$ ($\alpha = 0.5$–1) in the variable of the abscissa, but also failed to collapse the data of various sets with $0.1 \leqslant P \leqslant 0.75$. Observe that scaling relations for the roughness and for related quantities are typically built to fit power laws, so it is not surprising that they fail to fit the apparently exponential relations obtained with the probability P [Eq. (19)].

IV. DISCUSSION

A. Summary of scaling regimes

Figure 13 illustrates the scaling regimes of the roughness that can be observed only with the kinetic barrier (which accounts for the hidden out-of-plane diffusion) and with the addition of a small ES barrier.

At short times, both plots show the oscillations characteristic of layer-by-layer growth, which are damped as the film grows. The damping is related to the formation of stable islands on the top of larger islands, which prevents the formation of flat surfaces for integer coverage θ. If the ES barrier is present, the hopping rates are reduced at all step edges, including monolayer steps, facilitating the nucleation at multiple layers; a quantitative treatment is in Ref. [36]. If the ES barrier is absent, the instability of islands with two adatoms seems to be a necessary condition for the oscillations; according to previous results of submonolayer growth, this is achieved if $\epsilon R^{2/3} \gtrsim 10$ [33,35].

If only the kinetic barrier is present, the layer-by-layer regime is followed by roughening in the VLDS class [11,12], i.e., the same universality class of the CV model without step edge barriers [13]. The roughness range of this regime is small, typically $0.5 \lesssim W \lesssim 3$, but the thickness range may be long (see data for set C and $P = 1$ in Fig. 13). The VLDS roughening leads to the formation of an increasing density of steps with height difference larger than 1, which activates the kinetic barrier and reduces the interlayer transport. This leads to a regime of unstable roughening, in which mounds nucleate and begin to grow and the local slopes of the $\log W \times \log \theta$ plots may reach values larger than 1. Finally, as the mounds become sufficiently high, the mass flux between them is suppressed (there is no mechanism of transient mobility of incident atoms in the model) and the convergence to SG is observed.

If an ES barrier is present, the difference is the absence of a transient VLDS regime. The restriction to interlayer transport is always active, even at monolayer steps, so the instability begins as soon as the layer-by-layer growth is suppressed. Indeed, the nucleation of mounds can be observed when $W \approx 1$, i.e., in very smooth surfaces.

The observation of these scaling regimes in simulation works and in real deposition processes strongly depends on the working temperature, which controls the adatom mobility (R, ϵ) and the hopping probability at step edges (P). Observe that four regimes are shown in set C with $P = 1$ (Fig. 13) because the simulations reached 10^5 layers; however, only two or three of those regimes are observed with the other parameter sets with $P = 1$ and deposition of 10^4 layers (which usually corresponds to thicknesses of a few micrometers). Moreover, with $P \leqslant 0.01$ ($E_{ES} \geqslant 4.6 k_B T$), our simulations show SG since early times. This explains the difficulties of previous works to determine universal behaviors in the presence of ES barriers, leading, e.g., to suggestions of continuously varying exponents for the roughness scaling (see Sec. IV C for relations with those works).

For quantitative studies of the crossovers between scaling regimes, a suitable quantity is the smooth film thickness θ_c,

defined as the thickness in which the roughness is equal to the diameter of an atom or molecule [Eq. (17)]. If VLDS scaling is observed at that point, it suggests that ES barriers are negligible. Instead, if the roughness is rapidly increasing at that point ($\beta_{\rm eff} \approx 0.5$ or larger), ES barriers are probably present. For small ES barriers, our simulations suggest an exponential dependence of θ_c on P if the other parameters are constant, which implies a high sensitivity to the ratio $E_{ES}/(k_BT)$. This may eventually be explored to estimate activation energies. Unfortunately, that type of exponential relation seems to prevent the incorporation of the parameter P in scaling laws, in contrast with the case without the ES barrier.

B. Possible applications

Several models of homoepitaxial growth of metal and semiconductor films have already shown the effects of step edge barriers on the scaling of surface correlations [6,7]. Thus, this section has a focus on recent works on heteroepitaxial growth which show scaling relations similar to those obtained here. Evidently, such comparison is possible only when the growth has lost the memory on the initial substrate pattern.

Recent studies of deposition of oxides [37] and sulfides [38], using different techniques, showed growth exponents $\beta \approx 0.5$. Their fits of $\log W \times \log \theta$ plots do not seem to be influenced by the inclusion of data from relatively thin films. Thus, in both cases, we believe that the results are indicative of large ES barriers.

In recent works on chemical bath deposition of CdS on glass [39] and electron beam evaporation of SnTe on quartz [40], estimates of growth exponents β near 0.8 were obtained. Concomitantly, the values of $1/z$ estimated from correlation lengths are smaller than β, meaning that those lengths grow slower than the height fluctuations. This is a signature of unstable growth and suggests the presence of small ES barriers, i.e., $E_{ES} \lesssim k_BT$ [compare, for instance, with our results in Figs. 10(b)–10(d) (insets with $\beta_{\rm eff} > 0.5$) and Fig. 11 (slowly increasing length λ)].

In thermal evaporation of tin phthalocyanine dichloride [41], the film structure changed according to the choice of the substrate. The films grown on Si were amorphous and, for roughness ≈2–4 nm, $\beta = 0.21 \pm 0.08$ was obtained. The films grown on glass were formed by triclinic crystallites and, for roughness ≈2–6 nm, $\beta = 0.48 \pm 0.07$ was obtained. The growth units are molecules with characteristic sizes larger than 1 nm, so those films are in a regime of relatively low roughness ($W \sim 1$ in units of the lattice constant). Notably, the smoothest films (amorphous) show an exponent very close to the VLDS value, while the roughest films (polycrystalline) show an exponent close to the SG value. Since the structures of those films are different, it is possible that different interactions appear during their growth. If so, our results suggest that ES barriers are present in the polycrystalline films, but are much smaller (possibly absent) in the amorphous ones.

Finally, in organic molecular beam deposition of DIP films on SiO_2 ($T = 120\,^\circ$C), Zhang *et al.* [19] showed a transition from layer-by-layer growth (roughness oscillations) to an approximately linear increase of the roughness with the thickness. A recent work shows that this transition can be explained by strong intermolecular interactions near the substrate [42]. However, a simpler alternative interpretation of that transition is suggested by our results with small ES barriers. For instance, Fig. 10(a) shows that a small ES barrier and a high adatom mobility may lead to damped roughness oscillations followed by an approximately linear increase (sets H–M). This occurs with the same lateral interactions between the molecules in different layers. Since the roughening is highly sensitive to the value of the ES barrier, another possible explanation for the transition is a slight increase of the ES energy as the DIP films reach a certain thickness.

C. Relations with previous models

A previous investigation of kinetic roughening with the kinetic barrier and the ES barrier also considered DF of the incident atoms [16]. For a single parameter set without the ES barrier, VLDS scaling for $W \lesssim 1$ was observed. However, with the ES barrier, $W \sim t^{1/3}$ was obtained at large thicknesses ($\theta \sim 10^4$), which is significantly different from the SG obtained here. That power law is probably a consequence of the DF mechanism, which may lead to mound coarsening [43–45]. Other mechanisms may also contribute to mound coarsening and slope selection when ES barriers are present, such as corner diffusion [45] and transient mobility of incident atoms [46,47]. However, none of these mechanisms was present in our simulations.

Some authors studied the scaling of height correlations with ES barriers (but without the kinetic barrier) in other lattice structures. In modeling Fe/Fe(100) deposition up to five layers and small roughness ($W \leqslant a$), Amar and Family [48] showed significant differences in the roughening by varying E_{ES} from 0 to 0.04 eV, which are small barriers. This parallels our observation of a high sensitivity of the roughening with the ES barrier. Simulations by Bartelt and Evans considering DF showed an initial roughness oscillation followed by a scaling $W \sim \theta^{0.18}$ and skewed height distributions [47], in agreement with experiments [49,50]. The VLDS class has growth exponent $\beta \approx 0.20$ [25] and skewed height distributions [14], so our results suggest the possibility of VLDS roughening in those films; such a suggestion is based on the assumption of universality because quantitative comparisons with our results are not possible.

In a model of Ag/Ag(100) film deposition up to 2×10^3 layers, Caspersen *et al.* [51] showed oscillatory roughness at small thicknesses ($\theta = 1$–10) followed by a rapid increase of the effective growth exponent $\beta_{\rm eff}$, beginning when $W \sim 1$ (in lattice units). That exponent reached peak values between 0.45 and 0.8, depending on the temperature. At the largest thicknesses, the roughening was slower, with $\beta_{\rm eff}$ converging to 0.25–0.3. These results also parallel those of our work, although the inclusion of additional relaxation mechanisms and the consequent mound coarsening will lead to smaller β.

Recently, Schneider *et al.* [15] studied the roughening and mound coarsening of films grown in simple cubic lattices with and without ES barriers, but considering mechanisms of downward transport of incident atoms. The simulations up to 10^3 layers revealed a variety of behaviors of the roughness when it varied in the narrow range ≈0.3–3 (in lattice units). The growth exponents β and the coarsening exponents n estimated from the long-time behavior had remarkable

dependence on the model parameters. Our results suggest that the investigated thickness ranges are near or at an unstable regime, which explains the exponent variability. However, quantitative comparisons are not possible because that work considered the relaxation of incident atoms.

Finally, we recall that the kinetic barrier (with or without the ES barrier) was already considered in limited mobility growth models [21] and in models of the initial stages of heteroepitaxial film deposition [17,18]. In the latter, the adatom diffusion coefficients on the substrate were much larger than those on the film surface. Thus, in simulations with relatively small thicknesses, the roughness and the correlations were strongly influenced by the initial conditions set by the film-substrate interaction. This prevented a systematic study of the effects of the kinetic barrier in those works.

V. CONCLUSION

We studied the Clarke-Vvedensky (CV) model of film growth in simple cubic lattices and solid-on-solid conditions considering Ehrlich-Schwoebel (ES) barriers for adatoms to cross step edges and an additional kinetic barrier related to the hidden off-plane diffusion at edges with heights larger than one lattice constant. The latter barrier follows the proposal of Ref. [16]. Kinetic Monte Carlo simulations were performed in a broad range of values of the diffusion-to-deposition ratio R, of the detachment probability ϵ, and of the probability P associated with the ES energy barrier.

In the growth without the ES barrier, four scaling regimes are identified: an approximately layer-by-layer growth at small thicknesses θ, in which the roughness shows damped oscillations with maxima $W \approx 0.5$ (in units of the lattice constant); a kinetic roughening regime in the VLDS class when $W \sim 1$; unstable roughening with mound nucleation and growth, in which local slopes β_{eff} of $\log W \times \log \theta$ plots reach values larger (possibly much larger) than 0.5; and asymptotic statistical growth (SG), $W = t^{1/2}$, because mass flux between the mounds is suppressed. However, in most simulations until $\theta = 10^4$ layers, only some of those regimes are observed: in low-temperature conditions, the instability develops at short times, while in high temperatures the roughness may never reach 1 and only the layer-by-layer and the VLDS regimes may be observed.

If the ES barrier is present, no evidence of a VLDS regime is found, but the other regimes may be observed. Again, low adatom mobility (low temperature) and high ES barriers suppress the initial layer-by-layer growth and possibly lead to SG when a small number of layers is deposited.

We defined the smooth film thickness θ_c at the point in which the roughness is equal to the diameter of an atom or molecule. If the roughness has VLDS scaling at that point, it suggests that ES barriers are negligible. Otherwise, if the roughness is rapidly increasing at θ_c, typically with $\beta_{eff} \gtrsim 0.5$, a small ES barrier ($E_{ES} \sim k_B T$) may be present. The simulations suggest that θ_c scales exponentially with $\sim P^{2/3}$ if the other parameters are kept fixed, which represents a high sensitivity to the parameter P.

The large number of crossovers observed in our simulations and their remarkable dependence on the model parameters explain why previous simulation studies could hardly show universal features in growth with ES barriers, except for the predicted asymptotic SG. From the perspective of applications, the discrimination of those scaling regimes may be important for the estimation of growth parameters such as the activation energies. Along these lines, we compared values of growth and dynamical exponents obtained in some recent experiments with our models and identified cases in which those barriers are expected to be negligible, small ($E_{ES} \sim k_B T$), or large. However, quantitative comparisons are usually difficult due to the simple features of the model and the fact that most of the materials of interest do not have a simple cubic lattice structure.

ACKNOWLEDGMENTS

F.D.A.A.R. acknowledges support from the Brazilian agencies CNPq (Grant No. 305391/2018-6), FAPERJ (Grants No. E-26/210.040/2020 and No. E-26/201.050/2022), and CAPES (Grant No. 88881.700849/2022-01). T.B.T.T. acknowledges support from CAPES (Grant No. PNPD20130933-31003010002P7).

APPENDIX A: UNCERTAINTIES IN THE SIMULATION DATA

The uncertainty of the roughness in each film thickness is given by the standard deviation of this quantity in the simulated samples. Figure 14(a) shows the roughness with the corresponding uncertainties in films grown with set C and $P = 1$, considering ten simulated samples. The size of the error bars hardly exceeds the thickness of the curve which was formerly shown in Fig. 6(b). The same is observed in the other sets with all values of P.

The uncertainties in the lengths ξ and λ are the standard deviations of the values of these quantities obtained from Eqs. (11) and (13) in different samples, respectively. Figure 14(b) shows those lengths with the corresponding uncertainties in films grown with set M and $P = 1$. This also illustrates the general trend that the uncertainties are smaller than the sizes of the data points.

APPENDIX B: ABSENCE OF FINITE-SIZE EFFECTS IN THE SIMULATION DATA

When the films have smooth surfaces, typically with $W \lesssim 5$, finite-size effects are absent if the position λ of the first

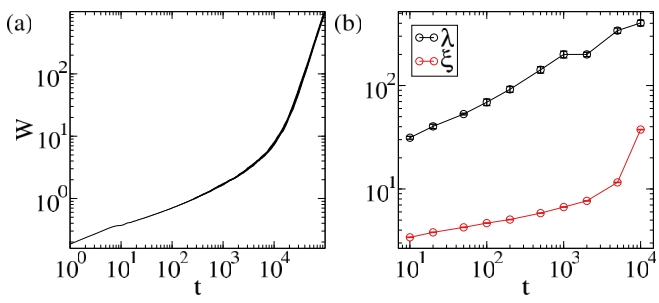

FIG. 14. (a) Surface roughness of films grown with set C and $P = 1$ with uncertainties. (b) Lengths ξ and λ of films grown with set M and $P = 1$ with uncertainties. All lengths are given in lattice units.

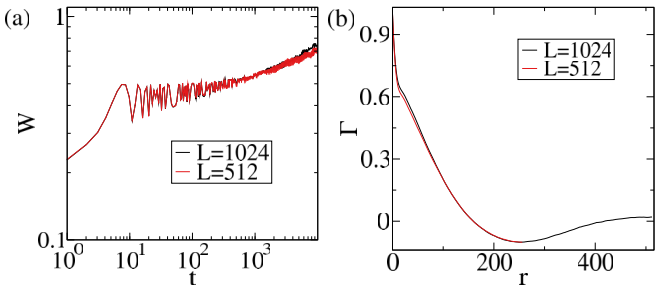

FIG. 15. (a) Surface roughness and (b) autocorrelation function of films grown with set K and $P = 1$ in lattice sizes $L = 512$ and $L = 1024$. All lengths are given in lattice units.

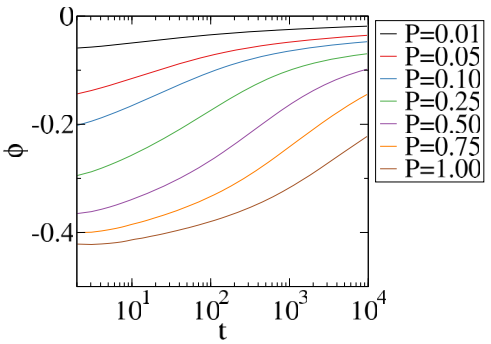

FIG. 16. Adatom current in films grown with set B and the indicated values of P. The lengths are in lattice units and the times are in units of $1/F$.

minimum of the autocorrelation function is smaller than $L/2$ (which is the maximal length in which spatial correlations can be calculated in systems with periodic boundaries). This is the same approach used in our previous simulations of films in the same thickness range [23,52]. The reliability of this method for set K with $P = 1$ is illustrated in Figs. 15(a) and 15(b) by comparing the roughness and the autocorrelation function, respectively, obtained in lattices with $L = 512$ and $L = 1024$. Observe that $\lambda \approx 250$ in those simulations, so $L = 512$ is the minimal length expected to provide size-independent results. Instead, in the lattice size used throughout this work ($L = 1024$), simulations with all sets from A to K obey a more rigid condition $\lambda \leqslant L/4$, which safely excludes the possibility of finite-size effects. Sets L and M with $P = 1$ are the only ones in which λ lies between $L/4$ and $L/2$.

When mounds are developed in the film surface (typically with $W \gtrsim 5$), lattice lengths much larger than λ are necessary to ensure that the observed structures are not affected by the lattice size. In these cases, we ensured that $|\Gamma(L/2)| < 0.05$; i.e., the correlations were very small at the maximal distances where they could be calculated. In these cases, we also obtained $\lambda < L/4$ and some comparisons of results in $L = 512$ and $L = 1024$ confirmed the absence of finite-size effects.

APPENDIX C: SUMMARY OF THE KMC ALGORITHM

The L^2 surface atoms have their positions (x, y) grouped into five lists $\{X_n\}$ according to the number of adatoms at nearest-neighbor sites ($n = 0, \ldots, 4$) at the same height z. The position of a surface particle in a list X_n is stored in an inverted-list matrix $M(x, y)$.

At each step of the simulation, the rates of all possible events (namely, deposition and hop of one of the L^2 surface particles) are calculated and their sum is denoted as Σ. The probability of a deposition event is the ratio between its rate and Σ. Since all particles in each list X_n have the same hopping rate, the probability of that list is the product of the number of particles in the list and the hopping rate divided by Σ. The event to be executed is then chosen according to those probabilities. In the case of choosing a list, one of its particles is randomly chosen to hop, in a direction which is also randomly chosen among four possibilities ($\pm x$, $\pm y$); in the case of a hop to a different layer, the hop is executed with probability P_{hop}, otherwise nothing occurs.

After a simulation step, the time is incremented by $1/\Sigma$ minus the natural logarithm of a randomly chosen number in the interval (0, 1]; the latter contribution has a very small effect on the total deposition time.

APPENDIX D: ADATOM CURRENTS

In a time interval Δt, the adatom current ϕ in the vertical direction is defined as the number of upwards movements minus the number of downwards movements of all surface atoms divided by $L^2 \Delta t$. Figure 16 shows the evolution of ϕ in films grown with set B and several values of P. In all cases, the current has negative values, which means that downward hops are more frequent than upward hops. This is expected because the sites with the highest coordinations are usually located at the lowest points. However, the monotonic increase of the current suggests that the upward and downward hops tend to be balanced at long times, thus leading to SG.

[1] M. Ohring, *Materials Science of Thin Films—Deposition and Structure*, 2nd ed. (Academic Press, New York, 2001).
[2] K. W. Kolasinski, *Surface Science: Foundations of Catalysis and Nanoscience*, 3rd ed. (John Wiley & Sons, Chichester, UK, 2012).
[3] A. E. Ares, *Thin Films* (IntechOpen, Rijeka, Croatia, 2021).
[4] G. Ehrlich and F. G. Hudda, J. Chem. Phys. **44**, 1039 (1966).
[5] R. L. Schwöebel, J. Appl. Phys. **40**, 614 (1969).
[6] T. Michely and J. Krug, *Islands, Mounds, and Atoms* (Springer, Berlin, 2003).
[7] J. W. Evans, P. A. Thiel, and M. C. Bartelt, Surf. Sci. Rep. **61**, 1 (2006).
[8] J. Krug, Adv. Phys. **46**, 139 (1997).
[9] S. Clarke and D. D. Vvedensky, J. Appl. Phys. **63**, 2272 (1988).
[10] A. Barabási and H. E. Stanley, *Fractal Concepts in Surface Growth* (Cambridge University Press, New York, 1995).
[11] J. Villain, J. Phys. I France **1**, 19 (1991).
[12] Z.-W. Lai and S. Das Sarma, Phys. Rev. Lett. **66**, 2348 (1991).
[13] T. A. de Assis and F. D. A. Aarão Reis, J. Stat. Mech.: Theory Exp. (2015) P06023.

[14] I. S. S. Carrasco and T. J. Oliveira, Phys. Rev. E **94**, 050801(R) (2016).
[15] J. P. Schneider, D. Margetis, F. Gibou, and C. Ratsch, J. Phys.: Condens. Matter **31**, 365301 (2019).
[16] F. F. Leal, S. C. Ferreira, and S. O. Ferreira, J. Phys.: Condens. Matter **23**, 292201 (2011).
[17] T. B. T. To, R. Almeida, S. O. Ferreira, and F. D. A. Aarão Reis, Appl. Surf. Sci. **560**, 149946 (2021).
[18] T. B. T. To and F. D. A. Aarão Reis, Surfaces **5**, 251 (2022).
[19] X. N. Zhang, E. Barrena, D. G. de Oteyza, and H. Dosch, Surf. Sci. **601**, 2420 (2007).
[20] E. E. M. Luis, I. S. S. Carrasco, T. A. de Assis, and F. D. A. A. Reis, Phys. Rev. E **102**, 012805 (2020).
[21] A. J. Pereira, S. G. Alves, and S. C. Ferreira, Phys. Rev. E **99**, 042802 (2019).
[22] Y. Zhao, G. Wang, and T. Lu, *Characterization of Amorphous and Crystalline Rough Surface: Principles and Applications* (Academic Press, San Diego, CA, 2001).
[23] I. S. S. Carrasco and T. J. Oliveira, Phys. Rev. Res. **2**, 013385 (2020).
[24] E. E. Mozo Luis, F. A. Oliveira, and T. A. de Assis, Phys. Rev. E **107**, 034802 (2023).
[25] F. D. A. A. Reis, Phys. Rev. E **70**, 031607 (2004).
[26] G. Ódor, B. Liedke, and K. H. Heinig, Phys. Rev. E **81**, 051114 (2010).
[27] H. Xia, G. Tang, Z. Xun, and D. Hao, Surf. Sci. **607**, 138 (2013).
[28] H. K. Janssen, Phys. Rev. Lett. **78**, 1082 (1997).
[29] C. A. Haselwandter and D. D. Vvedensky, Europhys. Lett. **77**, 38004 (2007).
[30] E. E. M. Luis, T. A. de Assis, and S. C. Ferreira, Phys. Rev. E **95**, 042801 (2017).
[31] T. B. T. To and F. D. A. A. Reis, J. Alloys Compd. **835**, 155093 (2020).
[32] C. Ratsch, P. Smilauer, A. Zangwill, and D. D. Vvedensky, Surf. Sci. **329**, L599 (1995).
[33] M. C. Bartelt, L. S. Perkins, and J. W. Evans, Surf. Sci. **344**, L1193 (1995).
[34] J. G. Amar and F. Family, Surf. Sci. **382**, 170 (1997).
[35] T. J. Oliveira and F. D. A. Aarão Reis, Phys. Rev. B **87**, 235430 (2013).
[36] J. Krug, P. Politi, and T. Michely, Phys. Rev. B **61**, 14037 (2000).
[37] J. A. Creeden, S. E. Madaras, D. B. Beringer, I. Novikova, and R. A. Lukaszew, AIP Adv. **9**, 095045 (2019).
[38] S. Rondiya, A. Rokade, A. Funde, M. Kartha, H. Pathan, and S. Jadkar, Thin Solid Films **631**, 41 (2017).
[39] I. Gupta and B. C. Mohanty, Sci. Rep. **6**, 33136 (2016).
[40] G. Maity, R. P. Yadav, R. Singhal, I. Sulania, A. K. Mittal, D. K. Chaudhary, D. Kanjilal, and S. P. Patel, J. Appl. Phys. **130**, 175306 (2021).
[41] S. Obaidulla and P. K. Giri, Appl. Phys. Lett. **107**, 221910 (2015).
[42] E. Empting, M. Klopotek, A. Hinderhofer, F. Schreiber, and M. Oettel, Phys. Rev. E **103**, 023302 (2021).
[43] J. G. Amar and F. Family, Phys. Rev. B **54**, 14742 (1996).
[44] M. Siegert and M. Plischke, Phys. Rev. E **53**, 307 (1996).
[45] J. G. Amar, Phys. Rev. B **60**, R11317 (1999).
[46] P. Šmilauer and D. D. Vvedensky, Phys. Rev. B **52**, 14263 (1995).
[47] M. C. Bartelt and J. W. Evans, Phys. Rev. Lett. **75**, 4250 (1995).
[48] J. G. Amar and F. Family, Phys. Rev. B **52**, 13801 (1995).
[49] Y. L. He, H. N. Yang, T. M. Lu, and G. C. Wang, Phys. Rev. Lett. **69**, 3770 (1992).
[50] J. A. Stroscio, D. T. Pierce, and R. A. Dragoset, Phys. Rev. Lett. **70**, 3615 (1993).
[51] K. J. Caspersen, A. R. Layson, C. R. Stoldt, V. Fournee, P. A. Thiel, and J. W. Evans, Phys. Rev. B **65**, 193407 (2002).
[52] T. B. T. To, V. B. de Sousa, and F. D. A. A. Reis, Physica A **511**, 240 (2018).